Magnesium Technology 2011
Edited by: Wim H. Sillekens, Sean R. Agnew, Neale R. Neelameggham, and Suveen N. Mathaudhu
TMS (The Minerals, Metals & Materials Society), 2011

Microstructure and Mechanical Behavior of Cast Mg AZ31B Alloy Produced by the Magnetic Suspension Melting Process

N.W. Rimkus, M.L. Weaver, N. El-Kaddah
The University of Alabama, Tuscaloosa, Alabama, USA

Keywords: Containerless Melting, Casting, Magnesium AZ31B alloy, Microstructure, Fracture

Abstract

Magnesium is the lightest of all structural metals and offers significant weight savings compared to traditional automotive materials. This paper describes the macrostructure and the microstructure of Mg AZ31B alloy produced via the Magnetic Suspension Melting (MSM) technique at a low superheat of 5°C. It was found that casting at this low superheat produced a fine globular grain structure in comparison to a dendritic structure in conventionally cast alloys. The intermetallic phases were analyzed in detail and compared with the conventionally cast alloy. In the MSM cast alloy, the $Mg_{17}Al_{12}$ phase formed mainly at the grain boundaries, in contrast to typical dendritic entrapment of this phase within the grains in conventional castings. The formation of the Al-rich secondary-α phase during solidification was investigated. The effects of this morphology change on mechanical and fracture behavior of this material are presented. These results are discussed relative to conventionally cast Mg alloys.

Introduction

With increasing demand for more fuel efficient automobiles, recent years have brought considerable interest in using cast magnesium components in vehicles. Magnesium will reduce weight, improving the fuel efficiency of automobiles [1,2]. Traditional AZ and AM series magnesium alloys are currently being used in low-strength applications such as steering wheels, instrument panels, air intake systems, and tank covers [1]. However, their use in structural applications such as: cross car beams, seat frames, steering column brackets, and vehicle front end structures have been rather limited due to contamination of the alloys during processing [1,3,4], macrosegregation and microsegregation [1,3], and the precipitation of intermetallic phases such as β-$Mg_{17}Al_{12}$ in the matrix and at the grain boundaries, all of which are known to be detrimental to the mechanical properties of these alloys [1,2,5,6].

Grain refinement in magnesium alloys has been a large focus in research in an effort to minimize the adverse effects of segregation and intermetallic precipitates on the mechanical properties. The addition of various grain refiners such as carbon and zirconium on the final grain structures have been extensively investigated [6,7,8]. These studies showed that the use of grain refiners can effectively reduce the grain size to about 20 μm, which is generally desirable to improve mechanical performance of the cast material [6,7]. For typical solidification rates in permanent mold and sand castings the grains are essentially dendritic, leading to entrapment of the aluminum-rich secondary-α phase between secondary dendrite arms [5,7]. Further improvement in the mechanical properties of the castings could be achieved by avoiding dendritic entrapment of the secondary-α phase by changing the solidification morphology to a globular one by way of another grain refinement method such as casting at low superheat [9,10,11,12].

The high reactivity of magnesium alloys makes contamination of the metal during melting in conventional melting systems unavoidable. The use of a protective SF_6 or CO_2-SF_6 gas to prevent magnesium burning only minimizes oxidation of the melt [13]. Furthermore, melting in a steel crucible leads to contamination with iron, which adversely affects grain refinement [8]. Therefore, the development of new melting technology that completely eliminates contamination would be highly desirable for casting magnesium structural automotive components.

The Magnetic Suspension Melting process (MSM), an integrated containerless induction melting and casting process, completely eliminates oxidation and contamination of the metal during melting. This is done by electromagnetically supporting the liquid metal in space. Previous work on melting and casting Al-Li alloys using this process at low superheat has yielded homogeneous, oxide free castings with a fine globular grain structures [10,11,12]. This paper examines low superheat castings of AZ31B produced by the MSM process. The microstructural features of MSM cast alloy are compared to those obtained at high superheat and the Charpy impact behavior of these castings are presented.

Experimental Technique

Figure 1 shows a schematic drawing of the experimental MSM system used in this study. It consists of two components: 1) an induction melting unit and 2) a casting chamber. The melting unit is basically an induction coil surrounding a silica tube with an inner diameter of 80 mm mounted on a stainless steel plate. The top of the tube is sealed using a brass flange fitted with ports for gas input and output and for a thermocouple. The charge material, which is a round billet 3" in diameter and 2" long, is placed on a water-cooled stainless steel chill block inside the silica tube. In this system, the induction coil is not stationary and moves during melting to maintain the containment force needed to support the molten metal. The motion of the coil is controlled using the laser tracking system.

The casting chamber is a cylindrical stainless steel tube attached to the chill plate of the melting unit. The casting mold is placed on the bottom plate of the casting chamber. In this work the mold was designed to allow unidirectional solidification of the melt. The mold is essentially an insulating refractory tube around a stainless steel chill plate located on the bottom. The refractory tube has a 3" ID and 3.5" OD, and a height of 6" made by Zircar Refractory. The stainless steel chill plate is 3" in diameter and 2" long. A thermocouple holder is placed on top of the refractory tube to allow measurements of the cooling rate along the mold

during solidification. Thermocouples are connected to an Omega TC-08 data acquisition system.

The entire system is sealed using O-rings, and is connected to a gas flow system which includes an argon gas cylinder and a vacuum pump. The induction coil, which surrounds the silica tube, has 10 turns and is connected to an Inductotherm 125 VIP power supply.

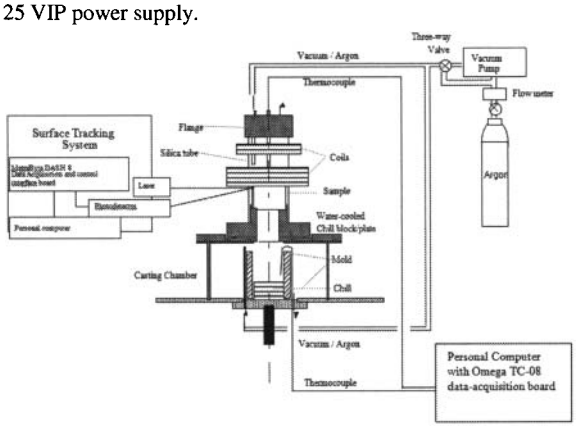

Figure 1. Schematic of the MSM experimental setup.

Casting experiments at high superheat were performed using conventional melting techniques. In these experiments the magnesium alloy was remelted in a steel crucible in a 1320 W resistance furnace under cover of CO_2-SF_6 gas. The molten metal was poured at 700 °C in the same mold used in the MSM experiments. The cooling curves along the mold during solidification were also measured using the Omega TC-08 data acquisition unit.

The melting and casting experiments were carried out using AZ31B magnesium alloy. The chemical composition of the alloy is shown is Table 1. Characterization of the castings include optical microscopy, scanning electron microscopy (SEM) and chemical analyses. The optical analysis was conducted on a Nikon Epiphot 200 Microscope with a SPOT Insight 2 camera attachment. SEM spectroscopy was conducted on a JEOL 7000 FEG SEM equipped with Oxford EDS and WDS systems. Microprobe analysis was conducted on a JEOL 8600 electron microprobe. This instrument was also equipped with a Si drift EDS system for rapid chemical mapping.

Impact toughness was assessed by means of room temperature Charpy impact tests. The specimens for impact testing were standard Charpy V-notch test bars with dimensions of 10 mm × 10 mm × 55 mm (V-notch depth = 2 mm) with their longitudinal directions parallel to the bottom of the mold.

Results and Discussion

This section presents results of characterization of unidirectional solidified AZ31B magnesium specimens prepared using the MSM process at low superheat of 5°C. The corresponding results for castings produced by conventional casting techniques at high superheat of 70°C are also presented.

Solidification Morphology and Grain Structure

Figures 2(a) and 2(b) show typical optical micrographs of the grain structure taken from the center of the ingot for the MSM and conventional castings respectively. These figures show that the grains of MSM cast alloy at 5°C superheat are much smaller than those obtained by conventional casting. The average grain size of the MSM cast alloy is 84μm while it is about 334 μm for the casting produced at high superheat of 70°C. It should be mentioned that there is very little variation in the grain size of the MSM cast ingot, despite the decrease in the solidification rate along the mold, away from the chill plate. Figure 2(a) also shows that the grain boundaries of the MSM casting are characterized by sharp interfaces, in contrast to the irregular grain boundaries observed in the conventional casting, Figure 2(b). The observed faceted interfaces in the MSM cast AZ31B suggests a plane front solidification morphology, which has been observed in Al alloys cast at such a low superheat [10,11].

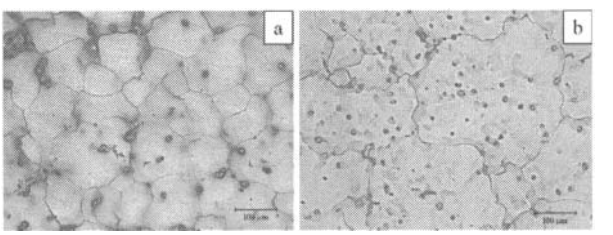

Figure 2. Optical micrographs of MSM (a) and conventionally cast (b) alloys etched using a Citric Acid solution .

Figures 3(a) and 3(b) show the morphologies of the grains produced at low and high superheat, respectively. The bright area corresponds to the primary α-Mg phase while the aluminum-rich secondary α-Mg phase appears dark. These figures show that the grains in the low superheat (i.e., MSM cast) alloy essentially consist of a primary-α phase with the secondary-α in the interstices between the grains; which is indicative of a globular solidification morphology, Figure 3(a), while it is dendritic at high superheat, Figure 3(b). At the solidification rate used in this investigation, the dendritic grains are equiaxed with the secondary-α phase between dendrite arms. The pronounced segregation of Al and other alloying elements within the equiaxed dendritic grains is the main source for the formation of the intermetallic phases observed within the matrix as shown in Figure 2(b). EDS mapping was conducted to confirm the segregation of aluminum in the grains. Figures 3(c) and 3(d) show the EDS aluminum maps for the grains produced at low and high superheat, respectively. Grain boundaries have been added in white showing that the aluminum rich secondary-α phase is found in the matrix between dendrite arms in the high superheat casting, Figure 3(d). Comparatively, the MSM low superheat casting, Figure 3(c), confirms the secondary-α phase is found along the grain boundaries only. This segregation explains the low superheat's lack of intermetallic phases appearing in the matrix.

The significant difference in the grain size and solidification morphology can be attributed to the high nucleation potential of the melt in the MSM process due to casting at low superheat [10]. This also acts to enhance the rate of grain growth and reduces the temperature gradient at the solidification front,

Table 1 Chemical Composition of AZ31B Ingot used in experiments

Magnesium	Aluminum	Silicon	Zinc	Nickel	Copper	Iron	Calcium	Manganese	OET
95.444%	3.140%	0.051%	0.661%	0.001%	0.001%	0.005%	0.020%	0.377%	0.300%

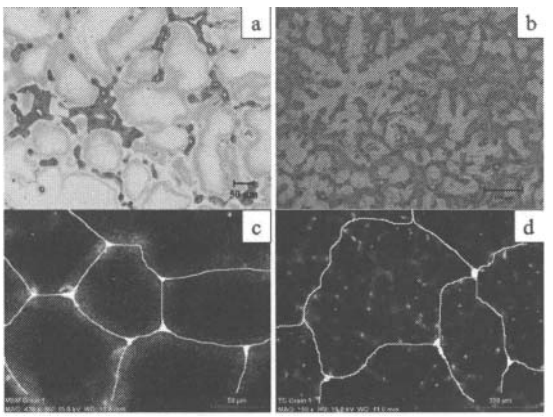

Figure 3. (a)Optical micrograph of the MSM casting showing a globular structure. (b) Optical micrograph of the conventional casting showing a dendritic structure. (c) EDS Map of Al for the MSM casting showing a globular structure. (d) EDS Map of Al for the conventional casting showing a dendritic structure.

thus favoring the transition from dendritic to globular solidification [15].

Intermetallics

The grain structure of the conventionally cast ingot, Figure 3(b), shows typical formation of the β-intermetallic particles in both the matrix and along the grain boundaries [5]. The distribution of the intermetallic precipitates shown in Figure 3 depends on the solidification morphology. For globular solidification morphology, corresponding to casting at low superheat in the MSM process, the intermetallic precipitates are found only at the grain boundaries. For dendritic solidification the precipitates are formed both within the grains as well as along the grain boundaries. This feature is attributed to the difference in the microsegregration of aluminum during solidification, Figure 3. For the globular solidification morphology, aluminum-rich liquid remains ahead of the solidification front rather becoming entrapped between the primary and secondary dendrite arms in dendritic solidification morphology.

The two main intermetallic phases formed in cast AZ31B alloys are β-$Mg_{17}Al_{12}$ and Al_8Mn_5. The β-$Mg_{17}Al_{12}$ phase is the most predominant precipitate in the castings. For casting at high superheat, the β-$Mg_{17}Al_{12}$ precipitates are found in two forms: (1) within the grains the β phase is formed as divorced or partially divorced particles, Figure 4(b); while (2) along the grain boundaries, in addition to the divorced and partially divorced particles, β-$Mg_{17}Al_{12}$ is present in a lamellar-type form. The formation of lamellar β phase occurs during the final stages of solidification

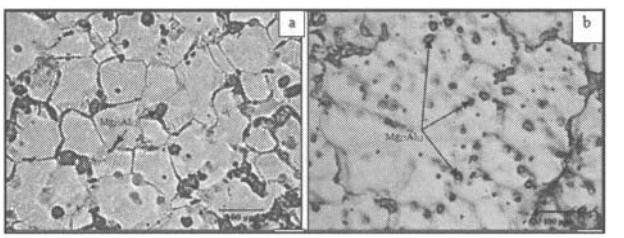

Figure 4. (a) Optical micrograph of the MSM casting showing $Mg_{17}Al_{12}$. (b) Optical micrograph of the conventional casting showing $Mg_{17}Al_{12}$

and is generated by grain boundary movement. In the MSM cast alloy, the β precipitates are mainly of the lamellar type and are found exclusively along the grain boundaries. The lamellae size and spacing in globular solidification is much larger than that for dendritic solidification. This may be attributed to the relatively large volume of the liquid between impinging equiaxed globular grains, and the low thermal gradient present in the liquid.

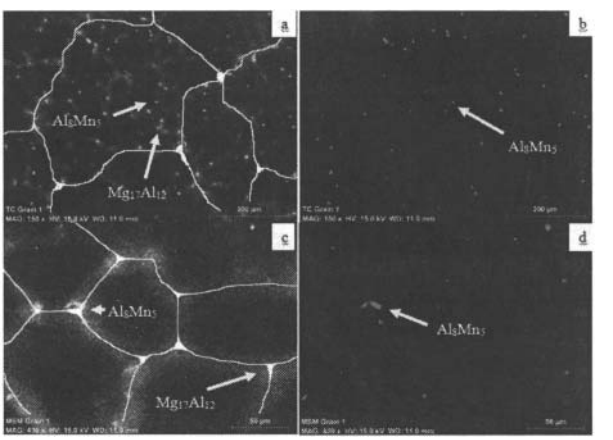

Figure 5. Al and Mn EDS Maps for (a,b) conventionally cast AM31B showing $Mg_{17}Al_{12}$ and Al_8Mn_5 phases. (c,d) EDS maps for MSM cast AM31B showing $Mg_{17}Al_{12}$ and Al_8Mn_5 phases along grain boundaries

Figure 5 shows EDS maps of aluminum (a,c) and manganese (b,d) for high and low superheats. These maps show overlapping Mn and Al dots where Al_8Mn_5 intermetallics are located. The EDS maps for the high superheat casting, Figures 5(a,b), show that the Al_8Mn_5 intermetallic is found both in the matrix as well as along the grain boundaries. The EDS maps for the low superheat casting, Figures 5(c,d), show that these intermetallics are only located along the grain boundaries. The EDS maps further support the occurrence of plane front solidification in the low superheat MSM castings.

Fracture Behavior

Charpy impact energies of 9.5 and 10 J were measured respectively for conventionally cast and MSM cast alloys. These values are equivalent to those for common Mg-Al-Zn alloys (i.e., 3 to 9 J) [16,17]. Figure 6 shows fracture surface images for the MSM and conventionally cast alloys. At low magnifications, the fracture surfaces for both castings exhibited large regions of quasi-cleavage decohesion with sizes corresponding to the grain sizes observed in each casting. Superimposed upon these regions were small cleavage facets and microshrinkage voids, arrowed in Figure 6(a), and ductile microvoids located within some of the Mg-rich solid solution regions. The small cleavage facets, which were associated with $Mg_{17}Al_{12}$ particles, and the microshrinkage voids appeared to act as fracture initiation sites within the conventional castings. Some similar features were observed in the

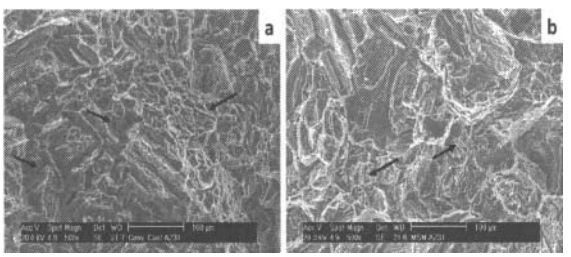

Figure 6 Fractographs (SEM) of (a) Conventionally Cast and (b) MSM cast impact toughness specimens.

MSM casting; however, the MSM casting contained no microshrinkage pores. Furthermore, the regions containing small cleavage facets were smaller and less numerous, and the percentage of microvoids was higher, suggesting a higher potential for plastic deformation.

Conclusions

Experiments were performed to investigate the solidification morphology and structure of AZ31B alloy cast at low superheats using the Magnetic Suspension Melting process. Casting at a superheat of 5°C was found to produce fine globular grains that were three times smaller than those obtained at a high superheat of 70°C. In the MSM casting, SEM/EDS analysis showed that the intermetallic precipitates were found exclusively at the grain boundaries. The main intermetallic precipitates in the cast ingot were β-$Mg_{17}Al_{12}$ and Al_8Mn_5. These results suggest that the MSM process may prove to be a viable technique to improve the properties for casting high strength magnesium automotive components.

Acknowledgments

The authors graciously thank the NSF for funding of this project under grant number CMMI-0856320

References

[1] N. Li, R. Osborne, B. Cox and D. Penrod, Magnesium Engine Cradle: The USCAR Structure Cast Magnesium Development Project: ASE paper, (2005) p. 337

[2] J.P. Thomson, S. Xu, M. Sadayappan, P.D. Newcombe, L. Millette, and M.Sahoo, Low Pressure Casting of Magnesium Alloys AZ91 and AM50: AFS Transactions, (2004) p. 1-10

[3] Soon Gi Lee, G.R. Patel, and A.M. Gokhale, Characterization of the effects of process parameters on macrosegregation in a high-pressure die-cast Magnesium alloy: Materials Characterization, (2005), V.55, p. 219-224

[4] Y. Chino, T. Furuta, M. hakamada, and M. Mabuchi "Influence of distribution of oxide contaminants on fatigue behavior in AZ31 Mg alloy recycled by solid-state processing," Materials Science and Engineering: A, V424 (2006) p. 355-360

[5] D.G. Leo Prakash, Doris Regener, "Quantitative characterization of $Mg_{17}Al_{12}$ phase and grain size in HPDC AZ91 Magnesium Alloy," Journal of Alloys and Compounds, V461 (2007) p. 139-146

[6] Q. Jin, J.-P. Eom, S.-G. Lim, W.-W. Park and B.-S. You, Grain Refining Mechanism of a Carbon Addition Method in a Mg-Al Magnesium Alloy: Scripta Materialia 49 (2003) 1129-1132.

[7] G. Han, X. Liu, and H. Ding, "Grain refinement of AZ31 magnesium alloy by new Al-Ti-C master alloys," Transactions of Nonferrous Metals Society of China, V19 (2009) p.1057-1064

[8] P. Cao, M. Qian, and D. H. StJohn, "Native grain refinement of magnesium alloys," Scripta Materialia, V53 (2005) p.841-844

[9] Frank Czerwinski, Near-liquidus molding of Mg-Al and Mg-Al-Zn alloys: Acta Materialia, (2005), V.53, p. 1973-1984

[10] J. Adams and N. Ei-Kaddah, Containerless processing and characterization of high purity aluminum alloys: in "Proceedings of the 1st International Conference on Processing Materials for Properties" (TMS, Warrendale, OH, 1993) p. 905-908.

[11] D. J. Reynolds, M. Shamsuzzoha and N. El-Kaddah, Characterization of Al-Li Castings Produced by the Magnetic Suspension Melting Process: in "Proceedings of the 4th Decennial International Conference on Solidification Processing", edited by J. Beech and H. Jones (Department of Engineering Materials, University of Sheffield, Sheffield, 1997) p. 45-48.

[12] C. Mahato, M. Shamsuzzoha and N. El-Kaddah, Solidification Morphology and Structure of Cast Al-Li 2090 Alloy at Low Superheats: in "Solidification of Aluminum Alloys", edited by M. G. Chu, D. A. Granger and Q. Han (TMS, Warrendale, OH, 2004) p. 321-328.

[13] H. Proffitt, "Magnesium and Magnesium Alloys," in "ASM Handbook on Casting" (ASM International, Materials Park, OH, 1988) p. 798.

[14] D.H. Kang, Manas Paliwal, Elhachmi Essadiqi, and In-Ho Jung, "Experimental Studies on the As-Cast Microstructure of Mg-Al Binary Alloys with Various Solidification Rates and Compositions," Magnesium Technology TMS, (2010) p.533-536

[15] Doru Michael Stefanescu, *Science and Engineering of Casting Solidification*, KA/PP, 2002, p.145-148

[16] H. W. Wagener, J. Hosse-Hartmann and R. Friz, "Deep Drawing and Impact Extrusion of Magnesium Alloys at Room Temparature," *Advanced Engineering Materials* 5 (2003) 237-242.

[17] J. Liao, M. Hotta, K. Kaneko and K. Kondoh, "Enhanced impact toughness of magnesium alloy by grain refinement," *Scripta Materialia* 61 (2009) 208-211.